Dynamics of soliton interaction solutions of the Davey-Stewartson I equation

Lijuan Guo,[1] Lei Chen,[1] Dumitru Mihalache,[2] and Jingsong He[3,*]

[1]*College of Science, Nanjing Forestry University, Nanjing, Jiangsu, 210037, People's Republic of China*

[2]*Department of Theoretical Physics, Horia Hulubei National Institute for Physics and Nuclear Engineering, 077125 Bucharest-Magurele, Romania*

[3]*Institute for Advanced Study, Shenzhen University, Shenzhen, Guangdong 518060, People's Republic of China*

(Received 15 July 2021; revised 6 December 2021; accepted 6 January 2022; published 31 January 2022)

In this paper, we first modify the binary Darboux transformation to derive three types of soliton interaction solutions of the Davey-Stewartson I equation, namely the higher-order lumps, the localized rogue wave on a solitonic background, and the line rogue wave on a solitonic background. The uniform expressions of these solutions contain an arbitrary complex constant, which plays a key role in obtaining diverse interaction scenarios. The second-order dark-lump solution contains two hollows that undergo anomalous scattering after a head-on collision, and the minimum values of the two hollows evolve in time and reach the same asymptotic constant value 0 as $t \to \pm\infty$. The localized rogue wave on a solitonic background describes the occurrence of a waveform from the solitonic background, quickly evolving to a doubly localized wave, and finally retreating to the solitonic background. The line rogue wave on the solitonic background does not create an extreme wave at any instant of time, unlike the one on a constant background, which has a large amplitude at the intermediate time of evolution. For large t, the solitonic background has multiple parallel solitons possessing the same asymptotic velocities and heights. The obtained results improve our understanding of the generation mechanisms of rogue waves.

DOI: 10.1103/PhysRevE.105.014218

I. INTRODUCTION

In mathematical physics, the Davey-Stewartson I (DS I) equation

$$\begin{aligned} &iu_t + u_{xx} + u_{yy} - 2\kappa|u|^2u + Su = 0, \\ &S_{xx} - S_{yy} = 4\kappa(|u|^2)_{xx}, \end{aligned} \tag{1}$$

where $\kappa = \pm 1$, u denotes the complex amplitude of a surface wave packet under gravity and surface tension, and S in this case is the velocity potential, was proposed first by Davey and Stewartson [1]. The DS I equation is the shallow water limit of the Benney-Roskes equation [2]. It arises in many physical applications, such as fluid dynamics [3–5], nonlinear optics [6], Bose-Einstein condensates [7], and plasma physics [8]. The DS I equation is a natural extension of the (2+1)-dimensional nonlinear Schrödinger equation, and it has been widely studied in recent years.

The N-soliton solutions of the DS I equation have been given by various authors [9–11]. In Ref. [10], Satsuma and Ablowitz also analyzed lump solutions through the "long wave" limit technique. The dromion-type solutions of the DS I equation were studied in various papers [12–16]. Also, Tajiri *et al.* investigated the interactions between periodic solitons and other types of solitons [17] and the existence of long-range interaction between two quasiline solitons through a periodic soliton [18]. More recently, special rational solutions were found by Ohta *et al.* [19] via the Hirota bilinear method, namely line rogue waves, which arise from the constant background with a line profile and disappear into the constant background again, which can be regarded as the limit of the spatial periodical solution [20]. He *et al.* [21] further studied hybrid solutions to the DS I equation. The multiple lump solutions, which correspond to distinct spectral parameters at a simple pole, are characterized by trivial interaction scenarios, i.e., they maintain their shapes and velocities unchanged after collision. Ablowitz *et al.* [22–25], Stepanyants *et al.* [26,27], and Estévez *et al.* [28–30] also analyzed higher-order lumps by using the inverse scattering transformation method. Manãs *et al.* used the Wronskian method to study higher-order lumps of DS II [31]. These higher-order lumps are associated with the higher-order pole at the same spectral parameter, and the interaction between such waveforms is nontrivial, in contrast to that associated with multiple lump solutions.

As is well known, the Darboux transformation (DT) is a very efficient tool to construct many kinds of exact solutions to soliton equations [32–39]. The binary DT (BDT) of the DS I equation has been constructed by Matveev [40] and Gu *et al.* [41], where they used 2×2 matrix solutions to analyze the one-fold Darboux transformation [see Eq. (6.1.22) in Ref. [40] and Eq. (2.71) in Ref. [41]]. But in order to obtain fundamental rational solutions such as the first-order lump and line rogue wave solutions, it is necessary to modify the BDT. In other words, the one-fold BDT should start with column vector solutions [see Eq. (A3) in Appendix A] instead of 2×2 matrix ones.

The term "rogue wave" refers to the transient gigantic ocean wave of extreme amplitude that appears from nowhere

*Corresponding author: hejingsong@szu.edu.cn, jshe@ustc.edu.cn

 ©2022 American Physical Society

and disappears without a trace [42]. Rogue waves have been responsible for a large number of maritime disasters [43]. Mathematically, the first-order rogue wave rational solution was first obtained for the $(1+1)$-dimensional nonlinear Schrödinger equation by Peregrine [44]. Rogue waves in $(1+1)$-dimensional integrable systems have been widely investigated both theoretically and experimentally [18,32,36,39,45–56]. The investigations of rogue wave models in higher dimensions, and the study of generating mechanisms of various kinds of rogue waves in different physical contexts, are necessary and important; see, for example, Refs. [57–61]. Recently, some rogue wave solutions have been obtained in $(2+1)$-dimensional integrable systems, such as the B-type Kadomtsev-Petviashvili equation [62], the asymmetrical Nizhnik-Novikov-Veselov equation [37,63], the multicomponent $(2+1)$-dimensional long-wave–short-wave resonance interaction system [64], and the DS II equation [65]. Therefore, it is natural to question whether for the DS I equation there exist localized rogue waves (or line rogue waves) on a solitonic background.

Therefore, in this paper, we limit our attention to solving the following problems:

(i) We modify the BDT to derive additional exact solutions of the DS I equation. The one-fold BDT should start with column vector solutions instead of 2×2 matrix ones of the Lax pair (compare Eqs. (A3) in Appendix A with Eq. (6.1.22) in Ref. [40] [or Eq. (2.71) in Ref. [41]]). Through n iterations, the n-fold BDT is constructed.

(ii) By using the above BDT, three types of soliton interaction solutions of the DS I equation are obtained, namely a higher-order lump, a localized rogue wave on a solitonic background, and a line rogue wave on a solitonic background. The dynamical properties of these soliton interaction solutions are analyzed and discussed in detail.

The paper is organized as follows. In Sec. II, we first modify BDT by beginning with column vector solutions instead of 2×2 matrix ones of the Lax pair in one-fold BDT, and we provide a uniform expression of n-fold BDT. In Sec. III, by using the above BDT, the first type of soliton interaction solutions of the DS I equation are obtained, namely higher-order lumps, which are expressed by rational function forms, and they exhibit a nontrivial interaction. In Sec. IV, the second type of soliton interaction solutions in terms of semirational function forms are derived, namely the lumps and doubly localized rogue waves on the background containing certain line solitons. In Sec. V, the third type of soliton interaction solutions are constructed, namely the line rogue waves on a solitonic background, and their dynamics are studied. The conclusion and a discussion of the obtained results are presented in the final section.

II. BINARY DARBOUX TRANSFORMATION

As mentioned above, the DS I equation is the compatibility condition of the following linear Lax pair:

$$\Psi_y = J\Psi_x + U\Psi, \quad \Psi_t = 2iJ\Psi_{xx} + 2iU\Psi_x + V\Psi \tag{2}$$

with

$$J = \begin{pmatrix} 1 & 0 \\ 0 & -1 \end{pmatrix}, \quad U = \begin{pmatrix} 0 & u \\ v & 0 \end{pmatrix},$$
$$V = \begin{pmatrix} (w+iQ)/2 & i(u_x+u_y) \\ i(v_x-v_y) & (w-iQ)/2 \end{pmatrix}, \tag{3}$$

where $\Psi = (\psi, \phi)^T$ (T denotes transpose hereafter), $u, v = \kappa u^*$ ($\kappa = \pm 1$) are complex functions (the asterisk $*$ represents complex conjugation), and $Q = -2\kappa|u|^2 + S$ is a real function. Here x, y, t are three independent variables. Next, we outline the necessary steps for the construction of new solutions via BDT. We consider the adjoint system

$$\Phi_y = \Phi_x J - \Phi U, \quad \Phi_t = -2i\Phi_{xx}J + 2i\Phi_x U + \Phi W, \tag{4}$$

where J, U are given by Eq. (3) and

$$W = \begin{pmatrix} -(w+iQ)/2 & i(u_x-u_y) \\ i\kappa(u_x^*+u_y^*) & -(w-iQ)/2 \end{pmatrix}.$$

The DS I equation (1) is also the compatibility condition $\Phi_{yt} = \Phi_{ty}$. One can find that when Ψ solves the Lax pair equations (2), then $\Phi = \Psi^\dagger$ (the superscript $\dagger$ represents the conjugate transpose hereafter) is the solution of the adjoint linear system (4). In what follows, we only focus on the $\kappa = -1$ case. Before proceeding, some Lemmas and Theorems are given to demonstrate the n-fold DT of the DS I equation in Appendix A.

III. THE HIGHER-ORDER LUMPS ON A CONSTANT BACKGROUND

Before constructing various solutions of the DS I equation, a family of solutions of the Lax pair are derived; for more details, see Appendix B. In this section, we shall use the BDT method to study higher-order rational lump solutions of the DS I equation, which exhibit anomalous interaction processes, i.e., the lumps undergo a large scattering angle after a head-on collision. The minimum values of these lumps evolve in time and approach the same asymptotic constant value 0 corresponding to that of the simple first-order lump as $t \to \pm\infty$.

A. The first-order lump

For simplicity, in what follows we set $a > 0$, $\lambda = \alpha + i\beta$, and $\mathrm{Re}\,\lambda = \alpha = 0$ without loss of generality of the solutions for the DS I equation.

With the choice of the following set of parameters in Eq. (B5):

$$\lambda_1 = -i\beta(0 < \beta < a), \quad n = 1, \quad k_1 = 1, \quad C_{11} = 0,$$

and considering the moving reference coordinate frame,

$$\widetilde{x} = x - \frac{2\sqrt{a^2-\beta^2}(a^2-2\beta^2)}{a^2-\beta^2}t, \quad \widetilde{y} = y \tag{5}$$

(in what follows, we will omit the sign " $\sim$ "), then the first-order lump solution is given by

$$u_{\mathrm{lump}}^{[1]} = a + \frac{4\beta^2}{a}\frac{N_1 - i\beta N_2}{D_1}, \tag{6}$$

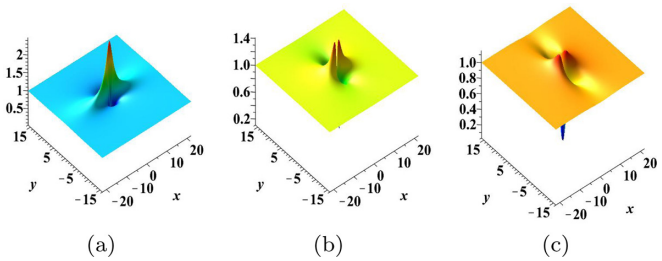

FIG. 1. The dynamical behavior of the intensity $|u^{[1]}_{\text{lump}}|$ of the first-order lump solution (6) with $a = 1$: (a) bright-lump solution: $\beta = \frac{\sqrt{7/2}}{2}$, (b) four-petal-lump solution: $\beta = \frac{\sqrt{2}}{2}$, (c) dark-lump solution: $\beta = \frac{1}{2}$.

where

$$N_1 = (\beta^2 - a^2)\left(\beta x + \frac{1}{2}\right)^2 - \beta^2\left(-\beta y + \frac{1}{2}\right)^2 + \frac{a^2}{4},$$
$$N_2 = [(a^2 - \beta^2)x^2 - \beta x + \beta^2 y^2 - \beta y]\sqrt{a^2 - \beta^2},$$
$$D_1 = 2(a^2 - \beta^2)\left(\beta x - \frac{1}{2}\right)^2 + 2\beta^2\left(\beta y - \frac{1}{2}\right)^2 + \frac{a^2}{2}.$$

Through simple calculations, the solution has the following properties:

(i) When $\frac{\sqrt{3}a}{2} \leqslant \beta \leqslant a$, the solution behaves as a bright-lump, as illustrated in Fig. 1(a).

(ii) When $\frac{a}{2} < \beta < \frac{\sqrt{3}a}{2}$, the solution behaves as a four-petal lump, as displayed in Fig. 1(b).

(iii) When $\beta \leqslant \frac{a}{2}$, the solution is a dark-lump, as shown in Fig. 1(c).

Remark 1. We always assume that $\text{Im}\,\lambda = -\beta < 0$ so that these integrals in Eq. (B5) converge.

Remark 2. To analyze the asymptotic properties of the higher-order dark lumps, we use the fact that the minimum value of the first-order dark lump is $\frac{a^2-4\beta^2}{a}$ at $(\frac{1}{2\beta}, \frac{1}{2\beta})$.

B. The second-order lump obtained by one-fold BDT

As mentioned above, we have obtained three types of lump solutions of the DS I equation. In this part of the article, we take a dark-lump ($0 < \beta \leqslant \frac{a}{2}$) solution as an example to further discuss the corresponding second-order solution, which is obtained by using one-fold BDT with the second-order Taylor coefficient [considering at the moving reference coordinate frame (5)].

With the selection of the following set of parameters in Eq. (B5):

$$\lambda_1 = -i\beta, \quad 0 < \beta \leqslant \frac{a}{2}, \quad n = 1, \quad k_1 = 2, \quad C_{11} = 0, \tag{7}$$

then the one-fold BDT yields a second-order dark-lump solution $u^{[2]}_{\text{lump}}$. Because of the cumbersome expression, we just give the used eigenfunction to analyze the dynamics of the solution:

$$\psi^{[2]} = -\frac{1}{(a^2 - \beta^2)^2}\left(F_r^{[2]} + F_I^{[2]}\right)\exp(\theta_2),$$
$$\phi^{[2]} = -\frac{3\mathrm{i}}{a(a^2 - \beta^2)^{\frac{3}{2}}}\left(G_r^{[2]} + G_I^{[2]}\right)\exp(\theta_2), \tag{8}$$

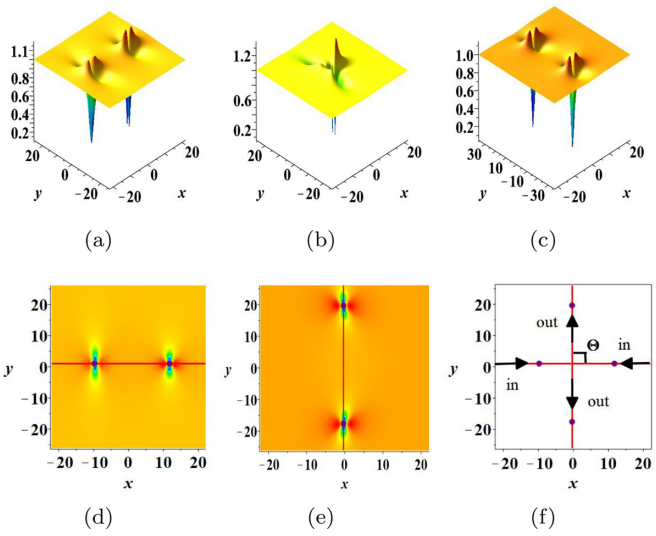

FIG. 2. The top panel: the time evolution process of the second-order dark-lump solution in Sec. III B with parameters $a = 1$, $\beta = \frac{1}{2}$ at (a) $t = -30$, (b) $t = 0$, and (c) $t = 30$. The bottom panel: the asymptotic dynamical behaviors: (d) $t = -30$, the red straight line $y = \frac{1}{2\beta}$, and the purple points are the positions of the minima of the two lumps; (e) $t = 30$, the red straight line $x = -\frac{\beta}{2\beta(a^2-\beta^2)}$, and the purple points are the positions of the minima of the two lumps; (f) the paths of the two pulses for the incoming ($t = -\infty$) and outgoing ($t = +\infty$) dynamics, with the scattering angle Θ indicated.

where

$$\theta_2 = \beta x + \sqrt{a^2 - \beta^2}iy - \frac{2\beta^3 t}{\sqrt{a^2 - \beta^2}},$$
$$F_r^{[2]} = -\frac{(a^2 - \beta^2)[(a^2 - \beta^2)x^2 - \beta^2 y^2]}{2} - \beta\sqrt{a^2 - \beta^2}(3a^2 - 2\beta^2)t,$$
$$F_I^{[2]} = \sqrt{a^2 - \beta^2}\left[(a^2 - \beta^2)\beta xy + \frac{1}{2}a^2 y\right],$$
$$G_r^{[2]} = \frac{(a^2 - \beta^2)^2 x^2}{6} + \frac{[\beta^2(a^2 - \beta^2)y + \beta(\beta^2 - a^2)]x}{3} + \frac{\beta^2(\beta^2 - a^2)y^2}{6} + \frac{\beta(3a^2 - 2\beta^2)y}{6} + \frac{(3a^2 - 2\beta^2)\sqrt{a^2 - \beta^2}\beta t}{3} - \frac{a^2}{6},$$
$$G_I^{[2]} = \left[-\frac{1}{6}(x - y)^2\beta^3 + \frac{(y - x)\beta^2}{3} + \frac{(x^2 - 2xy)a^2\beta}{6} + \frac{a^2(2x - y)}{6}\right]\sqrt{a^2 - \beta^2} - \frac{\beta^2(2\beta^2 - 3a^2)t}{3}.$$

Figure 2 (see the top panel) illustrates that this solution consists of two localized dark lumps along one straight line parallel to the x-axis that are well separated as $t \ll 0$; these two lumps become attracted to each other and overlap when $t \sim 0$, and then they separate as $t \gg 0$ but along the other straight line parallel to the y-axis. To investigate the two-dark-lump interaction, the hollow locations and heights need to be

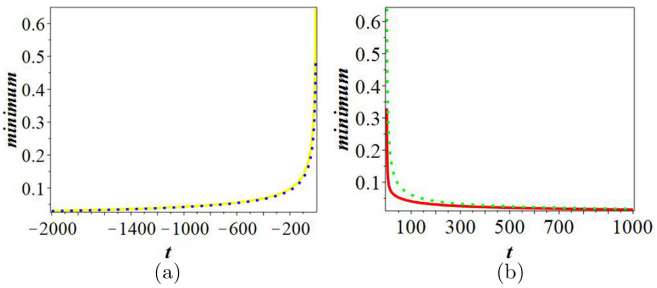

FIG. 3. (a) The minimum values of two lumps with parameters $a = 1,\ \beta = \frac{1}{2}$ before interaction; (b) the minimum values of two lumps with parameters $a = 1,\ \beta = \frac{1}{2}$ after interaction.

determined. The exact coordinates from the local minimum value of the second-order lump is too complicated to obtain, so we use an asymptotic analysis method to give approximate estimates. When the leading terms of the denominator of the second-order lump vanish, the approximate coordinates of two hollows are given as follows as $t \to -\infty$:

$$x = \pm\frac{\sqrt{-2\sqrt{a^2-\beta^2}\beta(3a^2-2\beta^2)t}}{a^2-\beta^2} + \frac{1}{2\beta}, \quad y = \frac{1}{2\beta}, \tag{9}$$

and when $t \to +\infty$ are approximately located at

$$x = -\frac{\beta}{2(a^2-\beta^2)},$$
$$y = \pm\frac{\sqrt{2\sqrt{a^2-\beta^2}\beta(3a^2-2\beta^2)t}}{\sqrt{a^2-\beta^2}\beta} + \frac{1}{2\beta}. \tag{10}$$

Based on the restriction $0 < \beta \leqslant \frac{a}{2}$ in Eq. (7), the inequalities $a^2-\beta^2 > 0,\ 3a^2-2\beta^2 > 0$ also hold. According to Eqs. (9) and (10), the two lumps move along two straight lines (i.e., $y = \frac{1}{2\beta}$ and $x = -\frac{\beta}{2(a^2-\beta^2)}$) with velocities $v_-(O(\pm 1/\sqrt{-t}), 0)$ and $v_+(0, O(\pm 1/\sqrt{t}))$; concretely the $+\infty$ line is obtained from the $-\infty$ line by the reflection on the x axis with an angle $\Theta = \pi/2$. They first accelerate to collide and then decelerate to move away from each other. Figure 2 (see the bottom plane) illustrates the asymptotic behaviors. It can be seen explicitly from that figure that the scattering angle is $\pi/2$. The approximate hollow locations are in good agreement with the exact ones, as shown by the density plot. The approximate hollow heights are also calculated by inserting these approximate coordinates (9) and (10) into the expression of the second-order lump solution. The minimum values of the two lumps evolve in time and finally approach 0 corresponding to that of the first-order dark lump (see Remark 2) as $t \to \pm\infty$, as seen in Fig. 3. Physically, we arrive at the conclusion that the two lumps undergo a nonelastic collision, i.e., though their amplitudes do not change, both the velocities and phases change a lot after interaction. This phenomenon also happens in other $(2+1)$-dimensional integrable systems, such as the KP I equation [22] and the DS II equation [25].

C. The second-order lump solution obtained by two-fold BDT

In this part of the article, we consider the other second-order lump that is obtained by using two-fold BDT and

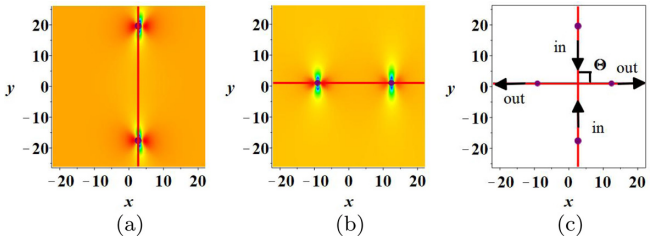

FIG. 4. The long-time asymptotic behavior of the second-order dark-lump solution obtained by the two-fold DT in Sec. III C, with parameters $a = 1,\ \beta = \frac{1}{2}$: (a) $t = -30$, the red straight line $x = \frac{3a^2-4\beta^2}{2\beta(a^2-\beta^2)}$, and the purple points are the positions of the two minima of the two lumps; (b) $t = 30$, the red straight line $y = \frac{1}{2\beta}$, and the purple points are the positions of the two minima of the two lumps; (c) the path of the two pulses for the incoming ($t = -\infty$) and outgoing ($t = +\infty$) dynamics, with the scattering angle Θ indicated.

choosing the first- and second-order Taylor coefficients as eigenfunctions. By contrast to the one in the above subsection, the solution shows an opposite dynamical evolution process.

For comparison with the second-order one in Sec. III B, we still analyze the dark-type lump case. With the selection of the following set of parameters in Eq. (B5):

$$\lambda_2 = \lambda_1 = -i\beta, \quad 0 < \beta \leqslant \frac{a}{2}, \quad n = 2,$$
$$k_1 = 1, \quad k_2 = 2, \quad C_{11} = C_{12} = C_{21} = C_{22} = 0 \tag{11}$$

and at the moving reference coordinate frame (5), the other second-order lump solution $\widetilde{u^{[2]}_{\text{lump}}}$ of the DS I equation is obtained. The explicit expression for $\widetilde{u^{[2]}_{\text{lump}}}$ is complicated, hence we omit it here. Similarly, when the domain leading terms of the denominator in this solution vanish, the asymptotic coordinates of the two minima of two lumps are located at

$$\begin{aligned} x &= \frac{3a^2-4\beta^2}{2\beta(a^2-\beta^2)}, \\ y &= \pm\frac{\sqrt{-2\sqrt{a^2-\beta^2}\beta(3a^2-2\beta^2)t}}{\sqrt{a^2-\beta^2}\beta} + \frac{1}{2\beta} \end{aligned} \qquad t \to -\infty, \tag{12}$$

and

$$\begin{aligned} x &= \pm\frac{\sqrt{2\sqrt{a^2-\beta^2}\beta(3a^2-2\beta^2)t}}{a^2-\beta^2} \\ &\quad + \frac{2a^2-3\beta^2}{2\beta(a^2-\beta^2)}, \qquad t \to +\infty, \\ y &= \frac{1}{2\beta}, \end{aligned}$$

where $\sqrt{2\sqrt{a^2-\beta^2}\beta(3a^2-2\beta^2)t}$ is well-defined under the constraint $0 < \beta \leqslant \frac{a}{2}$. Similarly, the two lumps first experience a head-on collision along one straight line parallel to the y-axis, and then they are quickly away from each other along the other straight line parallel to the x-axis, as shown in Fig. 4. Comparing these results with those shown in Fig. 2, it is clearly seen that we get the time-reversed dynamical evolution

of the second-order lump obtained by the one-fold DT. One can obtain similar hollow height results to those given above; we do not repeat them here in detail. We point out that this interesting behavior does not occur in $(1+1)$-dimensional integrable systems.

Remark 3. The above investigated physical phenomena and the associated evolution dynamics also occur in the case of two other lump-type solutions: the four-petal and bright-lump solutions.

Remark 4. The nth-order lump can be obtained by the n-fold BDT with n eigenfunctions that are chosen by the kth ($k = 1, 2, \ldots, n$)-order Taylor coefficients or the one-fold BDT with one eigenfunction that is chosen by the nth-order Taylor coefficient. The former lump is the time-backward evolution of the latter one.

IV. LOCALIZED ROGUE WAVES ON A SOLITONIC BACKGROUND

In the above section, we mainly discussed the higher-order rational lump solutions of the DS I equation under the assumption $C_{ij} = 0$. From now on, when this constraint is not imposed, semirational solutions of the DS I equation containing lumps or localized rogue waves on a solitonic background are obtained. Their dynamical properties are also studied and discussed.

A. The dynamics of interaction between one lump and one line soliton

With the selection of the following set of parameters in Eq. (B5):

$$\lambda_1 = -i\beta(0 < \beta < a), \quad n = 1, \quad k_1 = 1, \quad C_{11} \neq 0,$$

this solution contains one lump and one line soliton and is obtained by the one-fold BDT,

$$u^{[1]}_{\text{lumps}} = a + \frac{4a\beta^3 i N_1}{D_1} \tag{13}$$

with

$$\begin{aligned} N_1 =& [-S^3x^2 - \beta^2 S y^2 + S\beta x + S\beta y \\ &+ i(S^2\beta x^2 + \beta^3 y^2 + S^2 x - \beta^2 y)]e^{\frac{2\beta(Sx-2\beta^2 t)}{S}}, \\ D_1 =& (S^2+\beta^2)\left[2S^2\left(\beta x - \frac{1}{2}\right)^2\right. \\ &\left. + 2\beta^2\left(\beta y - \frac{1}{2}\right)^2 + \frac{a^2}{2}\right]e^{\frac{2\beta(Sx-2\beta^2 t)}{S}} + 2S^2a^2\beta^3 C_{11}, \\ S =& \sqrt{a^2-\beta^2}. \end{aligned}$$

The solution is regular when $\beta C_{11} > 0$. Here, we concentrate on the case of $0 < \beta \leqslant \frac{a}{2}, C_{11} = \frac{1}{\beta}$. The waveform consists of a lump solution localized on a line solitonic background. When $t \to -\infty$, one lump interacts with a line soliton. As time progresses, the lump is gradually annihilated by the line soliton, and just the line soliton remains visible when $t \to +\infty$, as is illustrated in Fig. 5.

By asymptotic analysis, the coordinate of the lump is fixed at $(x = \frac{1}{2\beta}, y = \frac{1}{2\beta})$, and by computing the partial derivative

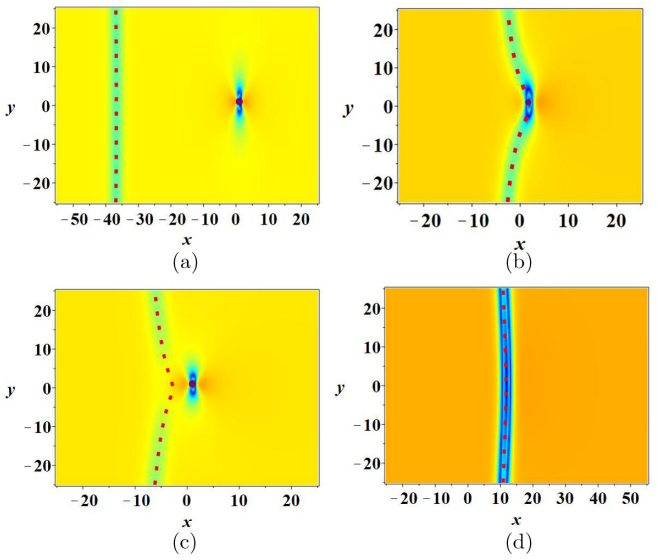

FIG. 5. The dynamical evolution of the fusion of a dark lump and a dark-line soliton with parameters $a = 1$, $C_{11} = \frac{1}{\beta}$, $\beta = \frac{1}{2}$. The purple points denote the positions of the lump $(x = \frac{1}{2\beta}, y = \frac{1}{2\beta})$, and the red dotted lines are given by the asymptotic curve Eq. (14) at different times. (a) $t = -50$, (b) $t = -6$, (c) $t = 0$, and (d) $t = 30$.

of this solution (13), the direction of the line soliton is approximately given by the curve

$$\begin{aligned} &\left\{(x,y) \in \mathcal{R}^2 : \frac{4\beta^3 t}{\sqrt{a^2-\beta^2}}\right. \\ &\left. = 2\beta x + \ln[(S^2x^2 + \beta^2 y^2)] - \ln(S^2\beta C_{11}), \quad x, y \to \infty\right\}. \end{aligned} \tag{14}$$

The direction is defined by the imaginary part of the spectral parameter $\lambda_{\text{Im}} = -\beta$, while the logarithmic curvature of the line soliton is induced by its interaction with the lump. In the asymptotic limit $|x| \to \infty$, Eq. (13) can be reduced to the form

$$u^{[1]}_{\infty} = a - \frac{2a\beta(\beta + iS)e^{\beta x - \frac{2\beta^3 t}{S}}}{a^2\left(e^{\beta x - \frac{2\beta^3 t}{S}} + C_{11}\beta e^{\frac{2\beta^3 t}{S} - \beta x}\right)} \tag{15}$$

with $C_{11}\beta > 0$ and $S = \sqrt{a^2-\beta^2}$. The field $u^{[1]}_{\infty}$ is the exact solution of the DS I equation and corresponds to a dark-line soliton along the direction $\beta x - \frac{2\beta^3 t}{S} = \text{const}$. From Fig. 5, we see that the asymptotic path given by Eq. (14) (red dotted line) shows good agreement with the analytical result illustrated by the density plot.

B. The first-order localized rogue wave on the background containing two dark-line solitons

With the choice of the following set of parameters in Eq. (B5):

$$\begin{aligned} &\lambda_2 = \lambda_1 = -i\beta(0 < \beta < a), \quad n = 2, \quad k_1 = 0, \\ &k_2 = 1, \quad C_{11} = C_{22} = C \neq 0, \quad C_{12} = C_{21} = 0, \end{aligned}$$

the first-order localized rogue wave on the background containing two line solitons is given by

$$u_{\rm rw}^{[1]} = a - \frac{\beta N_{\rm rw}}{a D_{\rm rw}}, \tag{16}$$

where

$$\begin{aligned} N_{\rm rw} =& S[2S\beta + i(S^2-\beta^2)]e^{2\beta x - \frac{4\beta^3 t}{S}} \\ &+ C\beta^3[S^2\beta x^2 + \beta^3 y^2 + S^2 x - \beta^2 y + S^2\beta \\ &+ i(S^3 x^2 + S\beta^2 y - S\beta x - S\beta y + S^3)], \\ D_{\rm rw} =& C\beta\left[S^2\left(\beta x - \frac{1}{2}\right)^2 + \beta^2\left(\beta y - \frac{1}{2}\right)^2 + \frac{a^2}{4} + S^2\beta^2\right] \\ &+ \frac{a^2}{4}e^{2\beta x - \frac{4\beta^3 t}{S}} + C^2 S^2 \beta^4 e^{-2\beta x + \frac{4\beta^3 t}{S}}, \\ S =& \sqrt{a^2-\beta^2}. \end{aligned}$$

When $t \to \pm\infty$, the solution only contains two parallel equal-amplitude line solitons. In the intermediate stage ($t \sim 0$), a remarkably localized wave lives for a short period of time and can reach the minimal value at a certain time. In this sense, we also term the localized wave as a *dark-rogue wave*. At the same time, the coordinates of the dark rogue wave are given by

$$x_0 = \frac{1}{2\beta}, \quad y_0 = \frac{1}{2\beta}, \tag{17}$$

and the dark-rogue wave approaches a minimum value 0.47 at an approximate time

$$t_0 = \frac{S\left[1 - \ln\left(\frac{4C\beta^3 S^2}{a^2}\right)\right]}{4\beta^3}. \tag{18}$$

Note that since the dark-rogue wave interacts with two line solitons, its minimum value is larger than the one (zero) of the first-order lump (see Remark 2). Meanwhile the two line solitons are given by the asymptotic curves

$$\begin{aligned} &\frac{4\beta^3 t}{S} = 2\beta x + \ln(S^2x^2 + \beta^2 y^2) - \ln(CS^2\beta), \\ &\qquad\qquad (x,y) \in \mathcal{R}^2. \\ &\frac{4\beta^3 t}{S} = 2\beta x - \ln(S^2x^2 + \beta^2 y^2) - \ln\left(\frac{4C\beta^3}{a^2}\right), \end{aligned} \tag{19}$$

These directions of the two line solitons are defined by $\lambda_{\rm Im} = -\beta$, while the logarithmic curvatures are induced by their interaction with the first-order lump. Equation (19) shows that the two line solitons are parallel and maintain velocities and shapes before and after collision. On the other hand, the two solitons do not overlap each other for the whole time, but in the intermediate stage of the evolution, since they exchange their intensities during collision, the localized dark rogue wave only lives for a short period of time. Because the localized rogue wave is emitted by the line soliton 1, it extracts energy from the line soliton, which results in a slight decrease of the intensity of the line soliton 1. The fusion of the localized rogue wave into the line soliton 2 increases its intensity. These two line solitons uniformly move along the positive direction of the x-axis for large space $r = \sqrt{x^2+y^2}$. Hence

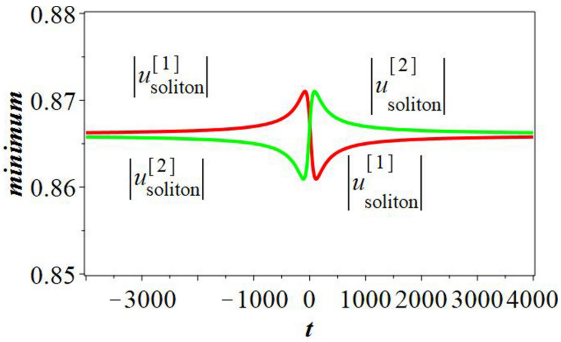

FIG. 6. The profiles along t of $|u^{[1]}_{\rm soliton}|$ (red solid line) and $|u^{[2]}_{\rm soliton}|$ (green solid line) with parameters $a = 1$, $\beta = \frac{1}{2}$ at $y = 100$.

we can consider the intensities of the two line solitons at $y = 100$. Along their centers (19), the solitons approximately attain the minimum value $\sqrt{a^2-\beta^2}$ as $t \to \pm\infty$, which is the minimum value of the exact dark-line soliton with the parameter $C = \frac{1}{\beta}$ of the DS I equation [see also Eq. (15)]. More precisely, inserting $y = 100$ into $u_{\rm rw}^{[1]}$ (16) and combining Eq. (19), the minimum values of the two line solitons with $a = 1$, $\beta = \frac{1}{2}$ are time-dependent but approach the same constant value corresponding to that of the first-order dark-line soliton $(|u^{[1]}_{\rm soliton}|_{\rm min}, |u^{[2]}_{\rm soliton}|_{\rm min}) \to (\frac{\sqrt{3}}{2}^+, \frac{\sqrt{3}}{2}^-)$ as $t \to -\infty$, and $(|u^{[1]}_{\rm soliton}|_{\rm min}, |u^{[2]}_{\rm soliton}|_{\rm min}) \to (\frac{\sqrt{3}}{2}^-, \frac{\sqrt{3}}{2}^+)$ as $t \to +\infty$; see Fig. 6. So the two line solitons keep their amplitudes unchanged after collision. For this localized wave, when $|t| > |t_0|$, the x-coordinate of the wave is affected due to interacting with line solitons. More specifically, the x-coordinate is obtained by solving the first equation of Eqs. (19) with $y = \frac{1}{2\beta}$ for $t > |t_0|$. With the choice of parameters $a = 1$, $\beta = \frac{1}{2}$, $C = 2$, its minimum value is time-dependent and approaches a constant 0.866 as $t \to +\infty$, as illustrated in Fig. 7(a). On the other hand, when $t < -|t_0|$, the x-coordinate is derived by solving the second equation of Eqs. (19) with $y = \frac{1}{2\beta}$. Similarly, with the selection of parameters $a = 1$, $\beta = \frac{1}{2}$, $C = 2$, its minimum value evolves in time and approaches a constant 0.866 as $t \to -\infty$, as illustrated in Fig. 7(b). It should be noted that the asymptotic minimum value of the localized wave is just the minimum value of two line solitons, which further confirms that the dark-rogue wave is nearly annihilated by two line solitons as $|t| \to \infty$. Figure 8 shows the whole dynamical process. It is clearly seen that the asymptotic curves

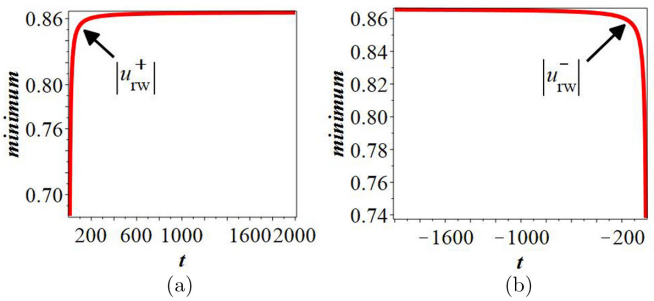

FIG. 7. The minimum value of $|u_{\rm rw}|$ along t ($-2000 < t < -10$, $10 < t < 2000$) with parameters $a = 1$, $\beta = \frac{1}{2}$, $C = 2$ at $y = 1$.

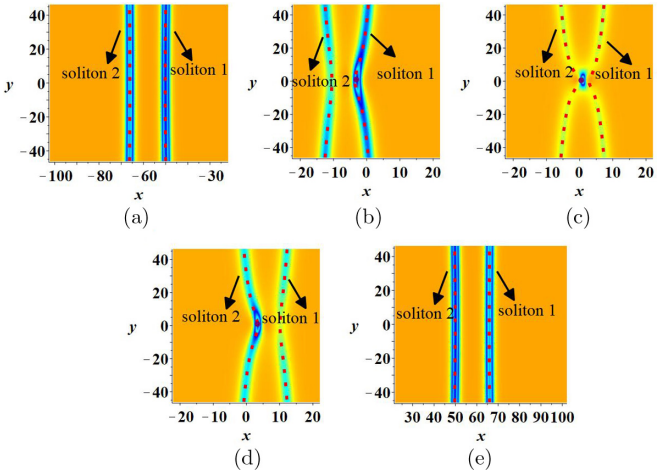

FIG. 8. The dynamical evolution process of the first-order localized rogue wave on the background containing two line solitons (16) with parameters $C = \frac{1}{\beta}$, $a = 1$, $\beta = \frac{1}{2}$. The red dotted curves denote the directions of the two line solitons (19), and the purple points present the positions of the localized wave. (a) $t = -100$, (b) $t = -10$, (c) $t = \sqrt{3}$, (d) $t = 10$, and (e) $t = 100$.

given by Eq. (19) (red dotted curves) are in good agreement with the exact analytical solution illustrated by the density plots for large values of space and time coordinates.

C. The second-order localized rogue wave on the background containing three dark-line solitons

With the choice of the following set of parameters in Eq. (B5):

$$\lambda_3 = \lambda_2 = \lambda_1 = -i\beta\left(0 < \beta \leqslant \frac{a}{2}\right), \quad n = 3,$$

$$k_1 = 0, \quad k_2 = 1, \quad k_3 = 2, \quad C_{11} = C_{22} = C_{33} \neq 0,$$

and other $C_{ij} = 0 (i \neq j)$, a second-order dark-rogue wave on the background containing three line solitons of the DS I equation is obtained. The solution and its asymptotic dynamics can be analyzed in the same manner as in the first-order localized dark-rogue wave case. Therefore, we omit most of the details and illustrate its dynamics via the density plot in Fig. 9, which shows that three line solitons move along the positive direction of the x-axis, interact with three holes, and annihilate them until just three line solitons are visible. When $|t| \to \infty$, the approximate curves of these three line solitons are located at

$$\begin{aligned}
\frac{4\beta^3 t}{S} &= 2\beta x + 2\ln[S^2x^2 + \beta^2 y^2 + 2\beta(3S^2 + \beta^2)t] \\
&\quad - \ln(4S^4), \\
\frac{4\beta^3 t}{S} &= 2\beta x - 2\ln[S^2x^2 + \beta^2 y^2 + 2\beta(3S^2 + \beta^2)t] \\
&\quad + 2\ln(4S^4), \\
\frac{4\beta^3 t}{S} &= 2\beta x, \quad S = \sqrt{a^2 - \beta^2}, \quad (x, y) \in \mathcal{R}^2. \qquad (20)
\end{aligned}$$

In the intermediate time, three dark lumps appear from the solitonic background, further evolve to a second-order localized dark-rogue wave, and decay again to the solitonic background. To be specific, we shall give the approximate traveling paths of localized waves below. When $t = 0$, the second-order localized dark-rogue wave is located at $(\frac{1}{2\beta}, \frac{1}{2\beta})$. When $t < 0$, the approximate coordinates of the three lumps satisfy the following equations, respectively:

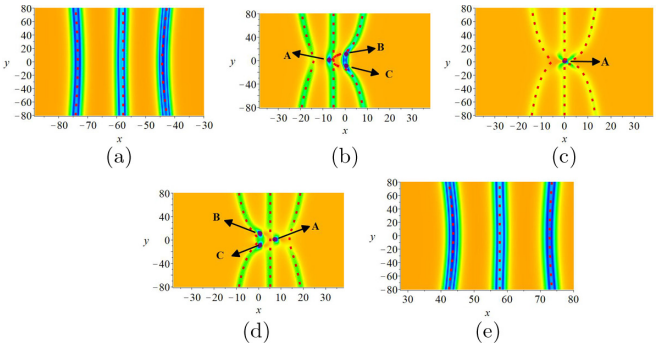

FIG. 9. The dynamical evolution process of the second-order rogue wave on the background containing three line solitons with parameters $C_{11} = C_{22} = C_{33} = \frac{1}{\beta}$, $a = 1$, $\beta = \frac{1}{2}$ in Sec. IV C. The red dotted curves denote the directions of the three solitons, and the purple points present the positions of the localized rogue wave and three localized lumps. (a) $t = -100$, (b) $t = -9$, (c) $t = 0$, (d) $t = 9$, and (e) $t = 100$.

$$\begin{aligned}
A: \quad & y = \frac{1}{2\beta}, \quad x = \frac{2\beta^2 t}{S} - \frac{1}{\beta}, \\
B: \quad & y = \frac{\sqrt{-2\sqrt{a^2 - \beta^2}\beta(3a^2 - 2\beta^2)t}}{\sqrt{a^2 - \beta^2}\beta} - \frac{1}{\beta}, \\
& 2\beta x = \frac{4\beta^3 t}{S} + 2\ln[S^2x^2 + \beta^2 y^2 + 2\beta(3S^2 + \beta^2)t] \\
& \quad - 2\ln(4S^4), \\
C: \quad & y = -\frac{\sqrt{-2\sqrt{a^2 - \beta^2}\beta(3a^2 - 2\beta^2)t}}{\sqrt{a^2 - \beta^2}\beta} - \frac{1}{\beta}, \\
& 2\beta x = \frac{4\beta^3 t}{S} + 2\ln[S^2x^2 + \beta^2 y^2 + 2\beta(3S^2 + \beta^2)t] \\
& \quad - 2\ln(4S^4), \quad (x, y) \in \mathcal{R}^2, \qquad (21)
\end{aligned}$$

where $-2\sqrt{a^2 - \beta^2}\beta(3a^2 - 2\beta^2)t > 0$ under these constraints $0 < \beta \leqslant \frac{a}{2}$ and $t < 0$.

When $t > 0$, the approximate coordinates of the three lumps satisfy the following equations, respectively:

$$\begin{aligned}
A: \quad & y = \frac{1}{2\beta}, \quad x = \frac{2\beta^2 t}{S} + \frac{1}{\beta}, \\
B: \quad & y = \frac{\sqrt{2\sqrt{a^2 - \beta^2}\beta(3a^2 - 2\beta^2)t}}{\sqrt{a^2 - \beta^2}\beta} + \frac{1}{\beta}, \\
& 2\beta x = \frac{4\beta^3 t}{S} - 2\ln[S^2x^2 + \beta^2 y^2 + 2\beta(3S^2 + \beta^2)t] \\
& \quad + \ln(4S^4),
\end{aligned}$$

$$C: \quad y = -\frac{\sqrt{2\sqrt{a^2-\beta^2}\beta(3a^2-2\beta^2)t}}{\sqrt{a^2-\beta^2}\beta} - \frac{1}{\beta},$$
$$2\beta x = \frac{4\beta^3 t}{S} - 2\ln[S^2x^2+\beta^2y^2+2\beta(3S^2+\beta^2)t] + \ln(4S^4), \quad (x,y)\in\mathcal{R}^2, \tag{22}$$

where $2\sqrt{a^2-\beta^2}\beta(3a^2-2\beta^2)t > 0$ under these constraints $0<\beta\leqslant\frac{a}{2}$ and $t>0$. The dynamical behavior is illustrated in Fig. 9. We see that the asymptotic results (the red dotted curves and the purple points) are in good agreement with the exact analytical ones illustrated by the density plots.

V. THE LINE ROGUE WAVES ON A SOLITONIC BACKGROUND

In this section, we discuss the fact that the line rogue wave solutions interact with line solitons of the DS I equation. The first- and second-order line rogue waves have been studied by Ohta and Yang in Ref. [19] by using the bilinear method. In what follows, to demonstrate the efficiency of the method used in the current work, apart from reporting novel results, we also review here some known results.

A. The interaction between the first-order line rogue wave and one dark-line soliton

Choosing the following set of parameters in Eq. (B5):

$$\lambda_1 = -i\beta(\beta>a>0), \quad n=1, \quad k_1=1, \quad C_{11}=0,$$

similarly to the first-order lump solution (6), a first-order fundamental line rogue wave of the DS I equation is obtained. The explicit expression and its dynamical evolution process are given in Appendix C. This solution is similar to the fundamental line rogue wave (3.1) in Ref. [19], hence we do not give the details.

Consequently, we focus on the case of $C_{11}\neq 0$. Then, a semirational solution containing a line rogue wave and a dark-line soliton is obtained:

$$u^{[1]} = a\left\{1-\frac{2\left[\left(sx+\beta y-\frac{1}{2}\right)^2+4(s^2+\beta^2)t^2-\frac{1}{4}-2i(s^2+\beta^2)t\right]}{\left(sx+\beta y-\frac{1}{2}\right)^2+4(s^2+\beta^2)t^2+\frac{1}{4}+\frac{C_{11}s^2a^2}{s-\beta}e^{2\beta x+2sy}}\right\} \tag{23}$$

with $s=\sqrt{\beta^2-a^2}$. Interacting with a line soliton, half of the first-order line rogue wave will be annihilated; see panel (b) in Fig. 10, corresponding to $t=0$. When $t\to\pm\infty$, the half-line rogue wave totally disappears and only the line soliton remains. By using asymptotic analysis, we find that the direction of the line soliton is given by the curve

$$\left\{(x,y)\in\mathcal{R}^2: 2\beta x+2sy = -\ln\left[\left(sx+\beta y-\frac{1}{2}\right)^2+4(s^2+\beta^2)^2t^2+\frac{1}{4}\right] + \ln\left(\frac{C_{11}s^2a^2}{\beta-s}\right)\right\} \tag{24}$$

with $s=\sqrt{\beta^2-a^2}$. This direction is defined by $\lambda_{\rm Im}=-\beta$ and the amplitude a, while the logarithmic curvature of the dark-line soliton is induced by its interaction with the line rogue wave. The complete time evolution is shown in Fig. 10.

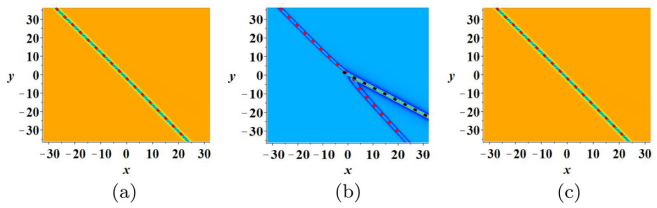

FIG. 10. The dynamical evolution of the interaction between a line rogue wave and a dark-line soliton with parameters $a=1$, $\beta=\sqrt{2}$, $C_{11}=\sqrt{2}-1$. The red dotted line represents the line soliton, and the black dotted line denotes the direction of the line rogue wave. (a) $t=-3$, (b) $t=0$, and (c) $t=3$.

The approximate results obtained for the directions of propagation are consistent with the exact analytical ones illustrated by the density plots. Here the red dotted line given by Eq. (24) represents the direction of propagation of the line soliton, and the black dotted line ($\beta y+sx-\frac{1}{2}=0$) denotes the direction of propagation of the dark-line rogue wave.

Remark 5. All solutions with parameters $\lambda=-i\beta$ ($\beta>0$) satisfy the property $|u(x,y,t)|=|u(x,y,-t)|$, hence in what follows we only show the dynamical evolution plots for negative time values.

B. The first-order line rogue wave on the background containing two dark-line solitons

With the choice of the following set of parameters in Eq. (B5):

$$\lambda_2=\lambda_1=-i\beta(\beta\geqslant a>0), \quad n=2, \quad k_1=0,$$
$$k_2=1, \quad C_{11}=C_{22}=C\neq 0, \quad C_{12}=C_{21}=0,$$

a first-order line rogue wave on the background containing two dark-line solitons is obtained. Unlike the first-order line rogue wave (C1) (see Appendix C), the solution does not show a short-lived large amplitude wave behaving as a straight line profile when $t=0$, but finally it also decays as $|t|\to\infty$ to two parallel dark-line solitons, constituting the solitonic background; see Fig. 11. Similar to the first-order localized dark-rogue wave on the background containing two line solitons discussed in Sec. IV, when the leading terms in the determinant of the solution vanish as $t\to\pm\infty$, the traveling paths of the two dark-line solitons are approximately

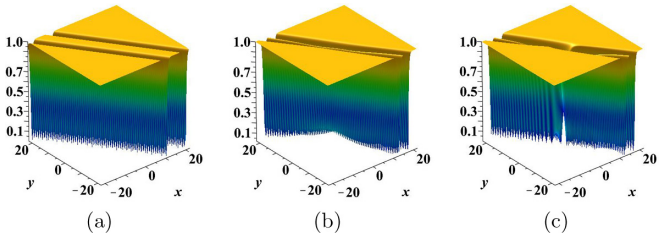

FIG. 11. The dynamical evolution of the first-order line rogue wave interacting with two dark-line solitons with parameters $a = 1$, $\beta = \sqrt{2}$, $C = \sqrt{2} - 1$: (a) $t = -100$, (b) $t = -1$, and (c) $t = 0$.

given by

$$
\begin{aligned}
(x, y) \in \mathcal{R}^2: \quad & \beta x + sy + \frac{1}{2}\ln\left[\left(sx + \beta y - \frac{1}{2}\right)^2\right. \\
& \left. + 4(s^2 + \beta^2)^2 t^2 + \frac{1}{4}\right] - \ln\left[\frac{Cs^2a^2}{\beta - s}\right] = 0, \\
& \beta x + sy - \frac{1}{2}\ln\left[(sx + \beta y - \frac{1}{2})^2\right. \\
& \left. + 4(s^2 + \beta^2)^2 t^2 + \frac{1}{4}\right] + \ln\left[\frac{Cs^2a^2}{2(\beta - s)}\right] = 0. \qquad (25)
\end{aligned}
$$

Equation (25) shows that the two line solitons approach two parallel straight lines for larger $r = \sqrt{x^2 + y^2}$, and when $|t| \gg 0$ the distance between the two line solitons is growing. For large space and time, the two line solitons possess the same amplitudes and velocities. Along their centers (25), and considering $y = 100$, the minimum values of the two line solitons (denoted $u^{[1]}_{\text{soliton}}$ and $u^{[2]}_{\text{soliton}}$, respectively) evolve in time and approach zero as $t \to \pm\infty$. We have pointed out in Remark 5 that these kinds of rational and semirational line rogue waves are all even functions with respect to variable t. We hence just show the minimum amplitudes of the two line solitons for large negative time, as seen in Fig. 12. Also, we see from Fig. 13 that the approximate trajectories given by Eq. (25) are in good agreement with the exact analytical results illustrated by the density plots.

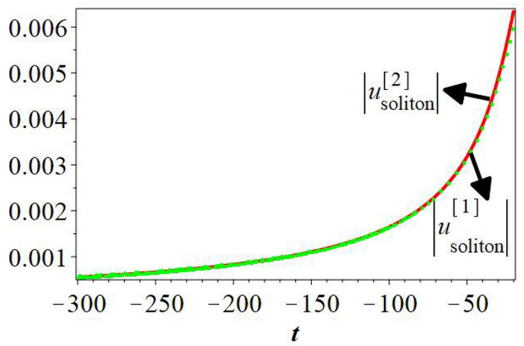

FIG. 12. The minimum value of $|u^{[1]}_{\text{soliton}}|$ (red solid line) and $|u^{[2]}_{\text{soliton}}|$ (green solid line) along t with parameters $a = 1$, $\beta = \frac{1}{2}$ at $y = 100$.

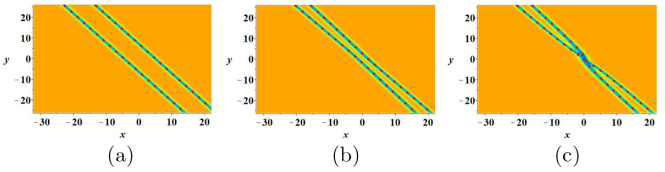

FIG. 13. The dynamical evolution of the first-order line rogue wave interacting with two dark line solitons with parameters $a = 1$, $\beta = \sqrt{2}$, $C = \sqrt{2} - 1$: (a) $t = -100$, (b) $t = -1$, and (c) $t = 0$.

C. The second-order line rogue wave on the background containing three dark-line solitons

With the choice of the following set of parameters in Eq. (B5):

$$
\begin{aligned}
& \lambda_3 = \lambda_2 = \lambda_1 = -i\beta, \quad \beta \geqslant a > 0, \quad n = 3, \quad k_1 = 0, \\
& k_2 = 1, \quad k_3 = 2, \quad C_{11} = C_{22} = C_{33} = C \neq 0,
\end{aligned}
$$

and other $C_{ij} = 0 (i \neq j)$, a second-order line rogue wave located at a three dark-line soliton background is obtained. Because of its cumbersome expression, here we just analyze its dynamical behavior. In contrast to the second-order line rogue wave shown in Fig. 4 of Ref. [19], when $|t| \to \infty$ the wave decays to the background containing three equal height and parallel dark line solitons. But, in the intermediate stage, due to the presence of three dark-line solitons, a large-amplitude parabola-shaped rogue wave does not occur. What is more, the approximate paths of the three dark-line solitons are given by the curves

$$
\begin{aligned}
& \beta x + sy - \ln\left[\left(sx + \beta y - \frac{1}{2}\right)^2 + 4(s^2 + \beta^2)^2 t^2 + \frac{1}{4}\right] \\
& \quad + \ln\left(\frac{1}{2}s^4a^2\right) = 0, \\
& \beta x + sy + \ln\left(\frac{1}{2}s^4a^2\right) = 0, \\
& \beta x + sy + \ln\left[\left(sx + \beta y - \frac{1}{2}\right)^2 + 4(s^2 + \beta^2)^2 t^2 + \frac{1}{4}\right] \\
& \quad + \ln\left(\frac{1}{2}s^4a^2\right) = 0, \quad (x, y) \in \mathcal{R}^2. \qquad (26)
\end{aligned}
$$

The corresponding dynamical evolution is shown in Fig. 14. The approximate expressions for the paths of the three dark-line solitons are consistent with the exact analytical ones illustrated by the density plots.

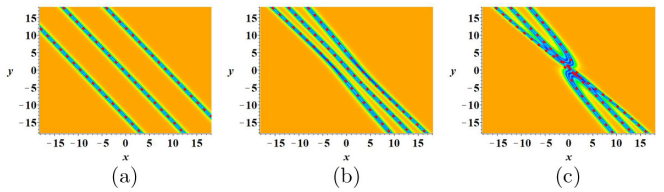

FIG. 14. The dynamical evolution of the second-order line rogue wave on a three-dark-line solitonic background with parameters $a = 1$, $\beta = \sqrt{2}$, $C = \sqrt{2} - 1$: (a) $t = -100$, (b) $t = -1$, and (c) $t = 0$. The red dotted lines denote the three approximate curves (26).

VI. CONCLUSION AND DISCUSSION

In this paper, the modified binary Darboux transformation has been used to construct a rich variety of exact solutions of the DS I equation, namely higher-order lumps, k-order localized rogue waves on a $k+1$ line solitons background, and k-order line rogue waves on a $k+1$ line solitons background. The higher-order lumps exhibit a nontrivial interaction, that is to say, the lumps first travel along one straight line, accelerate, and experience a head-on collision, after which they are scattered and rotated at a certain scattering angle, and then they move away from each other along the other direction, which is orthogonal to their initial trajectory. Their minimum values evolve in time and approach a constant 0 as $t \to \pm\infty$. A train of solitons possessing equal eigenvalues could evolve to a hugely localized wave; we termed these solutions as localized rogue wave on certain a line soliton background. What is more, the asymptotic trajectories and intensities of lumps and solitons have been estimated, and the obtained approximate results are in good agreement with the exact analytical ones. The minimum values of lumps approach the minimum values of line solitons as $t \to \pm\infty$, which confirms that these localized waves are indeed annihilated by these line solitons for a long time. On the other hand, for the line rogue wave on a certain line soliton background, because of the interaction with dark-line solitons, no large-amplitude waves appear at any instant of time.

The obtained results extend our understanding of the diversity and generation mechanisms of rogue waves. In addition, the method developed in this work could also be used in other $(2+1)$-dimensional integrable models, such as the $(2+1)$-dimensional asymmetric Nizhnik-Novikov-Veselov system [37], the Kadomtsev-Petviashvili equation, and other nonlinear evolution equations that are widely used to describe the dynamical evolution of diverse physical systems.

ACKNOWLEDGMENTS

This work is supported by the National Natural Science Foundation of China (Grants No. 12071304 and No. 12101312), the Natural Science Foundation of Jiangsu Province of China (Grant No. BK202110606), and the Natural Science Foundation of the Jiangsu Higher Education Institutions of China (Grant No. 21KJB110030).

APPENDIX A: n-FOLD BDT

Lemma 1. Suppose Ψ_1 and Ψ are two special column vector solutions of the Lax pair equations (2) corresponding to spectral parameters λ_1 and λ, respectively. Then we can have the following 1-closed differential form:

$$\omega(\Psi_1^\dagger, \Psi) = \Psi_1^\dagger \Psi\, dx + \Psi_1^\dagger J\Psi\, dy + 2i(\Psi_1^\dagger U\Psi + \Psi_1^\dagger J\Psi_x - \Psi_{1x}^\dagger J\Psi)dt. \tag{A1}$$

In addition, we have

$$\Omega(\Psi_1^\dagger, \Psi) = \int_{-\infty}^{x} \Psi_1^\dagger \Psi dx' + C, \tag{A2}$$

where C is a complex constant.

Following the ideas of Refs. [66–69], we obtain that the one-fold BDT for the DS I equation (1) is

$$\Psi \to \Psi[1] = \Psi - \frac{\Psi_1 \Omega(\Psi_1^\dagger, \Psi)}{\Omega(\Psi_1^\dagger, \Psi_1)},$$
$$U \to U[1] = U + [J, \Psi_1 \Omega(\Psi_1^\dagger, \Psi_1)^{-1} \Psi_1^\dagger]. \tag{A3}$$

Remark 6. Comparing Eq. (6.1.22) in Ref. [40] and Eq. (2.71) in Ref. [41], in the present work, the one-fold BDT (A3) is constructed by the column vector solution instead of the 2×2 matrix of the Lax pair.

The following conclusion verifies the validity of the above transformation (A3).

Theorem 1. Suppose Ψ solves the Lax pair equations (2), and Ψ_1 is a special solution corresponding to the spectral parameter λ_1. Then

$$\Psi[1]_y = J\Psi[1]_x + U[1]\Psi[1],$$
$$\Psi[1]_t = 2iJ\Psi[1]_{xx} + 2iU[1]\Psi[1]_x + V[1]\Psi[1]. \tag{A4}$$

Proof. For the first equation of (A4), by Lemma 1, it follows that

$$\begin{aligned}
\Psi[1]_x =& \Psi_x - \Psi_{1x}\Omega^{-1}(\Psi_1^\dagger, \Psi_1)\Omega(\Psi_1^\dagger, \Psi) \\
&+ \Psi_1\Omega^{-1}(\Psi_1^\dagger, \Psi_1)\Psi_1^\dagger\Psi_1\Omega^{-1}(\Psi_1^\dagger, \Psi_1)\Omega(\Psi_1^\dagger, \Psi) \\
&- \Psi_1\Omega^{-1}(\Psi_1^\dagger, \Psi_1)\Psi_1^\dagger\Psi, \\
\Psi[1]_y =& \Psi_y - \Psi_{1y}\Omega^{-1}(\Psi_1^\dagger, \Psi_1)\Omega(\Psi_1^\dagger, \Psi) \\
&+ \Psi_1\Omega^{-1}(\Psi_1^\dagger, \Psi_1)\Omega_y(\Psi_1^\dagger, \Psi_1)\Omega^{-1} \\
&\times (\Psi_1^\dagger, \Psi_1)\Omega^{-1}(\Psi_1^\dagger, \Psi) \\
&- \Psi_1\Omega^{-1}(\Psi_1^\dagger, \Psi_1)\Omega_y(\Psi_1^\dagger, \Psi) \\
=& J\Psi_x + U\Psi - (J\Psi_{1x} + U\Psi_1)\Omega^{-1}(\Psi_1^\dagger, \Psi_1)\Omega(\Psi_1^\dagger, \Psi) \\
&+ \Psi_1\Omega^{-1}(\Psi_1^\dagger, \Psi_1)\Psi_1^\dagger J\Psi_1\Omega^{-1}(\Psi_1^\dagger, \Psi_1)\Omega(\Psi_1^\dagger, \Psi) \\
&- \Psi_1\Omega^{-1}(\Psi_1^\dagger, \Psi_1)\Psi_1^\dagger J\Psi \\
=& J[\Psi_x - \Psi_{1x}\Omega^{-1}(\Psi_1^\dagger, \Psi_1)\Omega(\Psi_1^\dagger, \Psi) \\
&+ \Psi_1\Omega^{-1}(\Psi_1^\dagger, \Psi_1)\Psi_1^\dagger\Psi_1\Omega^{-1}(\Psi_1^\dagger, \Psi_1)\Omega(\Psi_1^\dagger, \Psi) \\
&- \Psi_1\Omega^{-1}(\Psi_1^\dagger, \Psi_1)\Psi_1^\dagger\Psi] \\
&- J\Psi_1\Omega^{-1}(\Psi_1^\dagger, \Psi_1)\Psi_1^\dagger\Psi_1\Omega^{-1}(\Psi_1^\dagger, \Psi_1)\Omega(\Psi_1^\dagger, \Psi) \\
&+ \Psi_1\Omega^{-1}(\Psi_1^\dagger, \Psi_1)\Psi_1^\dagger J\Psi_1\Omega^{-1}(\Psi_1^\dagger, \Psi_1)\Omega(\Psi_1^\dagger, \Psi) \\
&+ J\Psi_1\Omega^{-1}(\Psi_1^\dagger, \Psi_1)\Psi_1^\dagger\Psi - \Psi_1\Omega^{-1}(\Psi_1^\dagger, \Psi_1)\Psi_1^\dagger J\Psi \\
&+ U[\Psi - \Psi_1\Omega^{-1}(\Psi_1^\dagger, \Psi_1)\Omega(\Psi_1^\dagger, \Psi)] \\
=& J\Psi[1]_x + [J, \Psi_1\Omega^{-1}(\Psi_1^\dagger, \Psi_1)\Psi_1^\dagger][\Psi \\
&- \Psi_1\Omega^{-1}(\Psi_1^\dagger, \Psi_1)\Omega(\Psi_1^\dagger, \Psi)] \\
&+ U[\Psi - \Psi_1\Omega^{-1}(\Psi_1^\dagger, \Psi_1)\Omega(\Psi_1^\dagger, \Psi)] \\
=& J\Psi[1]_x + \{U + [J, \Psi_1\Omega^{-1}(\Psi_1^\dagger, \Psi_1)\Psi_1^\dagger]\} \\
&\times [\Psi - \Psi_1\Omega^{-1}(\Psi_1^\dagger, \Psi_1)\Omega(\Psi_1^\dagger, \Psi)] \\
=& J\Psi[1]_x + U[1]\Psi[1].
\end{aligned}$$

It is straightforward to verify the expression for $U[1]$ by using the symmetry relation. Thus, the first equation of (A4) has been proved. Similarly, one can verify the second equation of (A4). This completes the proof. ■

Based on Lemma 1 and Theorem 1, the first-fold BDT between old and new solutions for the DS I equation is explicitly given by

$$u^{[1]} = u + \frac{2\psi_1\phi_1^*}{\Omega(\Psi_1^\dagger, \Psi_1)}, \tag{A5}$$

where $\Psi_1 = (\psi_1, \phi_1)^T$ is a column vector solution to the Lax pair equations associated with the old potential solution u, meanwhile

$$\Omega(\Psi_1^\dagger, \Psi_1) = \int_{-\infty}^{x} (|\psi_1|^2 + |\phi_1|^2)dx' + C_{11},$$

with C_{11} being an arbitrary complex constant. We will next find that this constant plays a crucial role in constructing various solutions to the DS I equation.

Theorem 2. Suppose we have n distinct solutions $\Psi_i s (i = 1, 2, \ldots, n)$ for the Lax pair Eqs. (2). Then the n-fold BDT gives the transformation between the fields as

$$U^{[n]} = U + [J, \Theta M^{-1}\Theta^\dagger], \tag{A6}$$

where

$$\Theta = [\Psi_1, \Psi_2, \ldots, \Psi_n],$$

$$M = \begin{bmatrix} \Omega(\Psi_1^\dagger, \Psi_1) & \Omega(\Psi_1^\dagger, \Psi_2) & \cdots & \Omega(\Psi_1^\dagger, \Psi_n) \\ \Omega(\Psi_2^\dagger, \Psi_1) & \Omega(\Psi_2^\dagger, \Psi_2) & \cdots & \Omega(\Psi_2^\dagger, \Psi_n) \\ \vdots & \vdots & \ddots & \vdots \\ \Omega(\Psi_n^\dagger, \Psi_1) & \Omega(\Psi_n^\dagger, \Psi_2) & \cdots & \Omega(\Psi_n^\dagger, \Psi_n) \end{bmatrix},$$

$$\Omega(\Psi_i^\dagger, \Psi_j) = \int_{-\infty}^{x} \Psi_i^\dagger \Psi_j dx + C_{ij}, \quad 1 \leqslant i, j \leqslant n,$$

and C_{ij} are arbitrary complex constants.

APPENDIX B: A FAMILY OF EIGENFUNCTION SOLUTIONS OF THE LAX PAIR EQUATIONS

Before constructing solutions of the DS I equation, we first give a family of solutions of the Lax pair. We begin with the plane-wave seeding solution,

$$u = -v^* = a\exp[i(bx + cy + dt)],$$
$$Q = b^2 + c^2 + d, \quad w = 0, \tag{B1}$$

where parameters a, b, c, d are real constants, and we assume that the solution of the Lax pair (2) has the following form:

$$\psi = a_1\exp[i(b_1x + c_1y + d_1t)],$$
$$\phi = a_2\exp[i(b_2x + c_2y + d_2t)], \tag{B2}$$

where parameters a_k, b_k, c_k, d_k $(k = 1, 2)$ are complex constants. Inserting (B1) and (B2) into the Lax pair, the following relationships between parameters are obtained:

$$b_2 = b_1 - b, \quad c_2 = c_1 - c, \quad d_2 = d_1 - d,$$
$$a_2 = -\frac{a_1b_1i - a_1c_1i}{a}, \quad c_1 = \frac{b+c}{2} \pm \frac{\sqrt{\Delta}}{2},$$
$$\Delta = 4a^2 + b^2 - 4bb_1 + 2bc + 4b_1^2 - 4cb_1 + c^2,$$
$$d_1 = \frac{b^2 + c^2 + d}{2} - bb_1 + bc_1 + cb_1 - 2b_1c_1 - cc_1.$$

In what follows, without the loss of the diversity of solutions, for simplicity we set $b = 0, c = 0, d = 0, a_1 = 1$. Then the fundamental eigenfunction (we refer to the usual exponential function as a fundamental eigenfunction satisfying the Lax pair associated with the eigenvalue b_1) becomes

$$\psi = \exp\left[i\left(b_1x \pm \sqrt{a^2 + b_1^2}y \mp 2b_1\sqrt{a^2 + b_1^2}t\right)\right],$$
$$\phi = \frac{i\left(\pm\sqrt{a^2 + b_1^2} - b_1\right)}{a} \times \exp\left[i\left(b_1x \pm \sqrt{a^2 + b_1^2}y \mp 2b_1\sqrt{a^2 + b_1^2}t\right)\right]. \tag{B3}$$

By performing the above eigenfunction $\Psi = (\psi, \phi)^T$, the Taylor series expansion is as follows:

$$\Psi(b_1 = \lambda + \epsilon) = \Psi^{[0]} + \Psi^{[1]}\epsilon + \Psi^{[2]}\epsilon^2 + \cdots + \Psi^{[n-1]}\epsilon^{n-1} + \Psi^{[n]}\epsilon^n + O(\epsilon^{n+1}), \tag{B4}$$

where λ is a complex parameter, $\Psi^{[k]} = \frac{1}{k!}\frac{\partial^k\Psi}{\partial b_1^k}|_{b_1=\lambda} (k = 1, 2, \ldots, n)$, and $\epsilon > 0$ is an infinitesimal constant. Then these Taylor coefficients $\Psi^{[k]}$ all satisfy the Lax pair (2) with the same initial seeding solution (B1).

Therefore, the expression of the new solution in Theorem 2 can be generalized as follows.

Theorem 3. Suppose we have n distinct solutions $\Psi_i s$ $(i = 1, 2, \ldots, n)$ for the Lax pair (2), and we expand them as in (B4). Then the n-fold BDT gives the transformation between the fields as

$$U^{[n]} = U + [J, \Theta M^{-1}\Theta^\dagger], \tag{B5}$$

where

$$\Theta = \left[\Psi_1^{[k_1]}, \Psi_2^{[k_2]}, \ldots, \Psi_n^{[k_n]}\right],$$

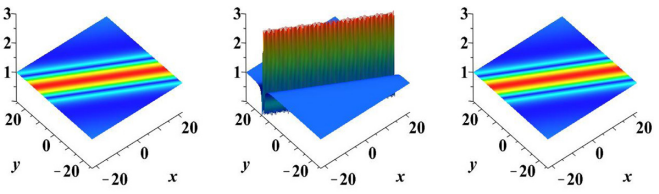

FIG. 15. The dynamical evolution of the first-order line rogue wave with parameters $a = 1$, $\beta = \sqrt{2}$, $C = \sqrt{2} - 1$: (a) $t = -3$, (b) $t = 0$, and (c) $t = 3$.

$$M=\begin{bmatrix} \Omega(\Psi_1^{[k_1]\dagger},\Psi_1^{[k_1]}) & \Omega(\Psi_1^{[k_1]\dagger},\Psi_2^{[k_2]}) & \cdots & \Omega(\Psi_1^{[k_1]\dagger},\Psi_n^{[k_n]}) \\ \Omega\left(\Psi_2^{[k_2]\dagger},\Psi_1^{[k_1]}\right) & \Omega\left(\Psi_2^{[k_2]\dagger},\Psi_2^{[k_2]}\right) & \cdots & \Omega\left(\Psi_2^{[k_2]\dagger},\Psi_n^{[k_n]}\right) \\ \vdots & \vdots & \ddots & \vdots \\ \Omega\left(\Psi_n^{[k_n]\dagger},\Psi_1^{[k_1]}\right) & \Omega\left(\Psi_n^{[k_n]\dagger},\Psi_2^{[k_2]}\right) & \cdots & \Omega\left(\Psi_n^{[k_n]\dagger},\Psi_n^{[k_n]}\right) \end{bmatrix},$$

$$\Omega\left(\Psi_i^{[k_i]\dagger},\Psi_j^{[k_j]}\right)=\int_{-\infty}^{x}\Psi_i^{[k_i]\dagger}\Psi_j^{[k_j]}dx'+C_{ij},$$

and C_{ij} are arbitrary constants.

APPENDIX C: THE FIRST-ORDER LINE ROGUE WAVE

The first-order line rogue wave is given by

$$u_{\mathrm{lrw}}^{[1]}=a\left[-1+\frac{1+4it(s^2+\beta^2)}{\left(sx+\beta y+\frac{1}{2}\right)^2+4(\beta^2+s^2)^2t^2+\frac{1}{4}}\right] \tag{C1}$$

with $s=\sqrt{\beta^2-a^2}$. Its typical dynamical evolution is shown in Fig. 15.

[1] A. Davey and K. Stewartson, On three-dimensional packets of surface waves, Proc. R. Soc. London, Ser. A **338**, 101 (1974).

[2] D. J. Benney and G. J. Roskes, Wave instability, Stud. Appl. Math. **48**, 377 (1969).

[3] V. D. Djordjevic and L. G. Redekopp, On two-dimensional packets of capillary-gravity waves, J. Fluid Mech. **79**, 703 (1977).

[4] M. J. Ablowitz and H. Segur, On the evolution of packets of water waves, J. Fluid Mech. **92**, 691 (1979).

[5] M. J. Ablowitz, *Nonlinear Dispersive Waves: Asymptotic Analysis and Solitons* (Cambridge University Press, Cambridge, 2011).

[6] M. J. Ablowitz, G. Biondini, and S. Blair, Nonlinear Schrödinger equations with mean terms in nonresonant multidimensional quadratic materials, Phys. Rev. E **63**, 046605 (2001).

[7] G. X. Huang, L. Deng, and C. Hang, Davey-Stewartson description of two-dimensional nonlinear excitations in Bose-Einstein condensates, Phys. Rev. E **72**, 036621 (2005).

[8] K. Nishinari, K. Abe, and J. Satsuma, A new-type of soliton behavior in a two dimensional plasma system, J. Phys. Soc. Jpn. **62**, 2021 (1993).

[9] D. Anker and N. C. Freeman, On the soliton solutions of the Davey-Stewartson equation for long waves, Proc. R. Soc. Lond. A **360**, 529 (1978).

[10] J. Satsuma and M. J. Ablowitz, Two-dimensional lumps in nonlinear dispersive systems, J. Math. Phys. **20**, 1496 (1979).

[11] M. Boiti, J. P. Leon, and F. Pempinelli, Multidimensional solitons and their spectral transforms, J. Math. Phys. **31**, 2612 (1990).

[12] M. Boiti, J. J. P. Leon, L. Martina, and F. Pempinelli, Scattering of localized solitons in the plane, Phys. Lett. A **132**, 432 (1988).

[13] A. S. Fokas and P. M. Santini, Coherent Structures in Multidimensions, Phys. Rev. Lett. **63**, 1329 (1989).

[14] A. S. Fokas and P. M. Santini, Dromions and a boundary value problem for the Davey-Stewartson I equation, Physica D **44**, 99 (1990).

[15] J. Hietarinta and R. Hirota, Multidromion solutions to the Davey-Stewartson equation, Phys. Lett. A **145**, 237 (1990).

[16] F. Guil and M. Mañas, Deformation of the dromion and solitonoff solutions of the Davey-Stewartson I equation, Phys. Lett. A **209**, 39 (1995).

[17] M. Tajiri, T. Arai, and Y. Watanabe, Resonant interactions of Y-periodic soliton with line soliton and algebraic soliton: Solutions to the Davey-Stewartson I equation, J. Phys. Soc. Jpn. **67**, 4051 (1998).

[18] M. Tajiri and T. Arai, Quasi-line interactions of the Davey-Stewartson I equation: On the existence of long-range interaction between two quasi-line solitons through a periodic soliton, J. Phys. A **44**, 235204 (2011).

[19] Y. Ohta and J. K. Yang, Rogue waves in the Davey-Stewartson I equation, Phys. Rev. E **86**, 036604 (2012).

[20] M. Tajiri and T. Arai, Growing-and-decaying mode solution to the Davey-Stewartson equation, Phys. Rev. E **60**, 2297 (1999).

[21] Y. B. Liu, C. Qian, D. Mihalache, and J. S. He, Rogue waves and hybrid solutions of the Davey-Stewartson I equation, Nonlin. Dyn. **95**, 839 (2019).

[22] M. J. Ablowitz and J. Villarroel, Solutions to the Time Dependent Schrödinger and the Kadomtsev-Petviashvili Equation, Phys. Rev. Lett. **78**, 570 (1997).

[23] J. Villarroel and M. J. Ablowitz, On the discrete spectrum of the nonstationary Schrödinger equation and multipole lumps of the Kadomtsev-Petviashvili I equation, Commun. Math. Phys. **207**, 1 (1999).

[24] M. J. Ablowitz, S. Chakravarty, A. D. Trubatch, and J. Villarroel A novel class of solutions of the non-stationary Schrödinger and the Kadomtsev-Petviashvili I equations, Phys. Lett. A **267**, 132 (2000).

[25] J. Villarroel and M. J. Ablowitz, On the discrete spectrum of systems in the plane and the Davey-Stewartson II equation, SIAM J. Math. Anal. **34**, 1253 (2003).
[26] K. A. Gorshkov, D. E. Pelinovskii, and Y. A. Stepanyants, Normal and anomalous scattering, formation and decay of bound-states of two-dimensional solitons described by the Kadomtsev-Petviashvili equation, Zh. Eksp. Teor. Fiz. **104**, 2704 (1993) [Sov. Phys. JETP **77**, 237 (1993)].
[27] W. C. Hu, W. H. Huang, Z. M. Lu and Y. A. Stepanyants, Interaction of multi-lumps within the Kadomtsev-Petviashvili equation, Wave Motion **77**, 243 (2018).
[28] P. G. Estévez, J. Prada, and J. Villarroel, On an algorithmic construction of lump solutions in a $2+1$ integrable equation, J. Phys. A **40**, 7213 (2007).
[29] J. Villarroel, J. Prada, and P. G. Estévez, Dynamics of lump solutions in a $2+1$ NLS equation, Stud. Appl. Math. **122**, 395 (2009).
[30] J. Villarroel, J. Prada, and P. G. Estévez, Weakly decaying solutions of nonlinear Schrödinger equation in the plane, J. Phys. A **50**, 495203 (2017).
[31] M. Mañas and P. Santini, Solutions of the Davey-Stewartson II equation with arbitrary rational localization and nontrivial interaction, Phys. Lett. A **227**, 325 (1997).
[32] B. L. Guo, L. M. Ling, and Q. P. Liu, Nonlinear Schrödinger equation: generalized Darboux transformation and rogue wave solutions, Phys. Rev. E **85**, 026607 (2012).
[33] P. Dubard and V. B. Matveev, Multi-rogue waves solutions: from the NLS to the KP-I equation, Nonlinearity **26**, R93 (2013).
[34] J. S. He, H. R. Zhang, L. H. Wang, K. Porsezian and A. S. Fokas, Generating mechanism for higher-order rogue waves, Phys. Rev. E **87**, 052914 (2013).
[35] J. S. He, L. H. Wang, L. J. Li, K. Porsezian, and R. Erdelyi, Few-cycle optical rogue waves: Complex modified Korteweg–de Vries equation, Phys. Rev. E **89**, 062917 (2014).
[36] L. J. Guo, L. H. Wang, Y. Cheng, and J. S. He, Higher-order rogue waves and modulation instability of the two-component derivative nonlinear Schrodinger equation, Commun. Nonlin. Sci. Numer. Simul. **79**, 104915 (2019).
[37] L. J. Guo, J. S. He, and D. Mihalache, Rational and semi-rational solutions to the asymmetric Nizhnik-Novikov-Veselov system, J. Phys. A **54**, 095703 (2021).
[38] Z. X. Zhou, Darboux transformation and global explicit solutions for nonlocal Davey-Stewartson I equation, Stud. Appl. Math. **141**, 186 (2018).
[39] S. H. Chen and D. Mihalache, Vector rogue waves in the Manakov system: Diversity and compossibility, J. Phys. A **48**, 215202 (2015).
[40] V. B. Matveev and M. A. Salle, *Darboux Transformations and Solitons* (Springer, Berlin, 1991).
[41] C. H. Gu, H. S. Hu, and Z. X. Zhou, *Darboux Transformation in Soliton Theory and Its Geometric Applications* (Science and Technology, Shanghai, 2005).
[42] N. Akhmediev, A. Ankiewicz, and M. Taki, Waves that appear from nowhere and disappear without a trace, Phys. Lett. A **373**, 675 (2009).
[43] C. Kharif, E. Pelinovsky, and A. Slunyaev, *Rogue Waves in the Ocean* (Springer, Berlin, 2009).
[44] D. H. Peregrine, Water waves, nonlinear Schrödinger equations and their solutions, J. Aust. Math. Soc. Ser. B **25**, 16 (1983).
[45] A. R. Osborne, M. Onorato, and M. Serio, The nonlinear dynamics of rogue waves and holes in deep-water gravity wave trains, Phys. Lett. A **275**, 386 (2000).
[46] N. Akhmediev, A. Ankiewicz, and J. M. Soto-Crespo, Rogue waves and rational solutions of the nonlinear Schrödinger equation, Phys. Rev. E **80**, 026601 (2009).
[47] Y. Ohta and J. Yang, General high-order rogue waves and their dynamics in the nonlinear Schrödinger equation, Proc. R. Soc. A **468**, 1716 (2012).
[48] D. R. Solli, C. Ropers, P. Koonath, and B. Jalali, Optical rogue waves, Nature **450**, 1054 (2007).
[49] A. Chabchoub, N. Hoffmann, M. Onorato, and N. Akhmediev, Super Rogue Waves: Observation of a Higher-Order Breather in Water Waves, Phys. Rev. X **2**, 011015 (2012).
[50] A. Chabchoub, N. Hoffmann, M. Onorato, A. Slunyaev, A. Sergeeva, E. Pelinovsky, and N. Akhmediev, Observation of a hierarchy of up to fifth-order rogue waves in a water tank, Phys. Rev. E **86**, 056601 (2012).
[51] J. S. He, L. J. Guo, Y. S. Zhang, and A. Chabchoub, Theoretical and experimental evidence of non-symmetric doubly localized rogue waves, Proc. R. Soc. A **470**, 20140318 (2014).
[52] A. Chabchoub and N. Akhmediev, Observation of rogue wave triplets in water waves, Phys. Lett. A **377**, 2590 (2013).
[53] F. Baronio, B. Frisquet, S. Chen, G. Millot, S. Wabnitz, and B. Kibler, Observation of a group of dark rogue waves in a telecommunication optical fiber, Phys. Rev. A **97**, 013852 (2018).
[54] M. Crabb and N. Akhmediev, Rogue wave multiplets in the complex Korteweg–de Vries equation, Rom. Rep. Phys. **72**, 118 (2020).
[55] A. Ankiewicz, M. Bokaeeyan, and W. Chang, Understanding general rogue wave solutions of the Gardner equation, Rom. Rep. Phys. **72**, 119 (2020).
[56] C. Hou, L. Bu, F. Baronio, D. Mihalache, and S. Chen, Sine-Gordon breathers and formation of extreme waves in self-induced transparency media, Rom. Rep. Phys. **72**, 405 (2020).
[57] N. Akhmediev, J. M. Dudley, D. R. Solli, and S. K. Turitsyn, Recent progress in investigating optical rogue waves, J. Opt. **15**, 060201 (2013).
[58] M. Onorato, S. Residori, U. Bortolozzo, A. Montina, and F. T. Arecchi, Rogue waves and their generating mechanisms in different physical contexts, Phys. Rep. **528**, 47 (2013).
[59] S. Chen, F. Baronio, J. M. Soto-Crespo, P. Grelu, and D. Mihalache, Versatile rogue waves in scalar, vector, and multidimensional nonlinear systems, J. Phys. A **50**, 463001 (2017).
[60] D. Mihalache, Localized structures in optical and matter-wave media: a selection of recent studies, Rom. Rep. Phys. **73**, 403 (2021).
[61] F. Selmi, S. Coulibaly, Z. Loghmari, I. Sagnes, G. Beaudoin, M. G. Clerc, and S. Barbay, Spatiotemporal Chaos Induces Extreme Events in an Extended Microcavity Laser, Phys. Rev. Lett. **116**, 013901 (2016).
[62] W. Q. Peng, S. F. Tian and T. T. Zhang, Analysis on lump, lumpoff and rogue waves with predictability to the

(2 + 1)-dimensional B-type Kadomtsev-Petviashvili equation, Phys. Lett. A **382**, 2701 (2018).

[63] P. X. Wu and Y. F. Zhang, Lump, lumpoff and predictable rogue wave solutions to the (2 + 1)-dimensional asymmetrical Nizhnik-Novikov-Veselov equation, Phys. Lett. A **383**, 1755 (2009).

[64] J. Rao, K. Porsezian, J. He, and T. Kanna, Dynamics of lumps and dark-dark solitons in the multi-component long-wave-short-wave resonance interaction system, Proc. R. Soc. A **474**, 20170627 (2018).

[65] L. J. Guo, J. S. He, L. H. Wang, Y. Cheng, D. J. Frantzeskakis, T. S. van den Bremer, and P. G. Kevrekidis, Two-dimensional rogue waves on zero background in a Benney-Roskes model, Phys. Rev. Research **2**, 033376 (2020).

[66] F. Guil and M. Mañas, Darboux transformations for the Davey-Stewartson equations, Phys. Lett. A **217**, 1 (1996).

[67] M. Mañas, Darboux transformations for the nonlinear Schrödinger equations, J. Phys. A **29**, 7721 (1996).

[68] A. Degasperis and S. Lombardo, Multicomponent integrable wave equations: I. Darboux dressing transformation, J. Phys. A **40**, 961 (2007).

[69] A. Degasperis and S. Lombardo, Multicomponent integrable wave equations: II. Soliton solutions, J. Phys. A **42**, 385206 (2009).